This is the Pre-Published Version.
H. Niu*, C. Chen, D. Ji, L. Li, Z. Li, Y. Liu, X. Huang* (2020) *Thermal-Runaway Propagation over a Linear Cylindrical Battery Module*. Fire Technology. https://doi.org/10.1007/s10694-020-00976-0
This is a post-peer-review, pre-copyedit version of an article published in Fire Technology. The final authenticated version is available online at: https://doi.org/10.1007/s10694-020-00976-0.

Thermal-Runaway Propagation over a Linear Cylindrical Battery module

Huichang Niu[*a], Caixing Chen[a], Dan Ji[a], Lei Li[a], Zhao Li[a], Yanhui Liu[b], Xinyan Huang[b,*]

[a]*Institute of Industry Technology, Guangzhou & Chinese Academy of Sciences, Guangzhou, 511458, China*

[b]*Department of Building Services Engineering, Hong Kong Polytechnic University, Kowloon, Hong Kong*

***Corresponding authors:** H. Niu niuhuichang@gziit.ac.cn and X. Huang xy.huang@polyu.edu.hk

Abstract*:* Thermal-runaway propagation in battery systems can escalate the battery fire hazard and pose a severe threat to global users. In this work, the thermal-runaway propagation over 18650 cylindrical Lithium-ion battery was tested in the linear-arranged module with a 3-mm gap. State of charge (SOCs) from 30% to 100%, ambient temperatures from 20 ℃ to 70 ℃, and three tab-connection methods were investigated. Results indicate that the thermal-runaway propagation speed was about 0.35 ± 0.15 #/min, which increased with SOC and ambient temperature. The critical surface temperature of thermal runaway ranged from 209 ℃ to 245 ℃, which increased with ambient temperature while decreased with SOC. Compared to the open-circuit module, the flat tab connection could cause an external short circuit to accelerate the thermal-runaway propagation, and the non-flat tab connection was more likely to trigger an explosion. A heat transfer analysis was proposed to qualitatively explain the speed and limiting conditions of thermal-runaway propagation, as well as the influence of SOC, ambient temperature, and tab connection. This work reveals the thermal-runaway propagation characteristics under well-controlled environments, which could provide scientific guidelines to improve the safety of the battery module and reduce battery fire hazards.

Keywords: Lithium-ion battery; thermal runaway; critical temperature; propagation speed; 18650 battery

Nomenclature

Symbols		**Abbreviations**	
A	heat transfer area (m^2)	ARC	adiabatic rate calorimeter
c	specific heat (J/kg-K)	EV	electric vehicle
E	electric energy (J)	LIB	Lithium-ion battery
h	heat transfer coefficient ($W/m^2/K$)	SOC	state of charge
m	mass (kg)	TC	thermocouple
n	number of cells (-)	TR	thermal runaway
Q	heat (J)		
$\dot{Q}$	heat release rate (W)	**Subscripts**	
r	propagation rate (#/min)	0	initial
R_t	total heat resistance (m^2/W)	a	ambient
t	time (min)	b	battery
T	temperature (°C)	es	external short circuit

1. Introduction

Lithium-ion batteries (LIBs) are widely used in electronic facilities and electric vehicles (EVs) for the merits of high energy density and long cycle life. However, fire or explosion hazards of LIBs initiated by the thermal runaway, when exposed to extreme conditions such as heat abuse, overcharge, crush, etc., present significant threats over lives [1–5]. Consequently, there is a big fire-safety concern on LIBs. Despite lots of understandings of the mechanism of thermal runaway and the developments of more stable LIB material systems over the last decade [6–9], it is still not possible to eliminate the risk of thermal runaway of LIBs. The propagation of thermal runaway from one cell to adjacent ones in battery packs and modules can escalate fire accidents of EVs and battery power storage facilities. Therefore, it is significant to understand the propagation dynamics of LIB thermal runaway from one cell to the whole battery pack, and the transition to fire, as a crucial step in the evolution of fire accidents.

So far, there has been a relatively limited number of studies on the thermal-runaway propagation of LIBs [10]. Some investigated the influence of battery arrangements and different dominating heat transfer processes. For modules with tightly packed prismatic LIBs, the heat conduction through the battery shell was considered as dominant because of the direct-contact and sandwich structure of the linearly arranged batteries [11–14]. Feng *et al*. [15] analyzed the thermal runaway induced by the mechanical penetration and the following propagation within a large battery module. They found that the heat transfer through the battery shell controlled the thermal-runaway propagation rate, while the heat conduction from the pole connector and heat radiation of fires had a much smaller influence. For battery modules with cylindrical LIBs, the dominant heat-transfer mechanism is more complex and unpredictable due to the matrix arrangement and cylindrical shape. Lopez *et al*. [16]estimated heat transfer rates between abused and adjacent cells at different spacings. They revealed the heat conduction of air to be dominant when battery space was 1 mm, while the heat conduction through nickel tabs became dominant when space was 2 mm until the meltdown of the welding between batteries and tabs.

Nevertheless, the propagation of thermal runaway within tightly packed LIB modules was not guaranteed, as observed for series-connected modules in [17–20]. The large heat dissipation to the environment contributes to the failed propagation, which could prevent LIB cells from reaching the critical thermal-runaway temperature [3]. Huang *et al*. [17] investigated the limiting conditions of LIB thermal runaway via a non-dimensional analysis and the combination of Semenov and Thomas models. They also demonstrated that both cell distance and ambient temperature affect the propagation of thermal runaway. Moreover, methods of connecting LIBs or the circuit arrangement also influence the thermal-runaway propagation process, because of the possible short circuit. Gao *et al*. [18] showed that for a close-circuit pouch-cell module, the cell temperature was 10 ℃ higher than the reference open-circuit module. Joshua *et al*. [19] showed that an intense thermal-runaway propagation occurred in the cylindrical-cell module with the parallel connection, while the propagation did not occur with the series connection. Therefore, further research is needed to further quantify the limiting conditions for the thermal-runaway propagation and determine the influence of the arrangement, state of charge (SOC), ambient temperature, and connection modes.

In this work, a series of experiments on the thermal-runaway propagation of LIB battery modules with 18650 cylindrical cells were conducted. The battery modules with six linearly arranged cells were tested, and the thermal-runaway propagation was initiated in one direction. Effects of ambient temperature, SOC, and the electric connection on thermal-runaway propagation were discussed in detail with a heat-transfer analysis. Experimental results aim to provide scientific guidelines for the safe design of cylindrical LIB modules.

2. Experimental Methods

2.1. Materials and setup

In this work, commercial 18650 Lithium-ion batteries (ICR18650-22P, Samsung SDI Co., Ltd) with the nominal capacity of 2150 mAh and nominal voltage 3.62 V were tested. The cathode and anode materials were $Li(Ni_{1/3}Co_{1/3}Mn_{1/3})O_2$ and graphite, respectively. The same batch of LIB cells from the same manufacturer was used in this study to minimize the influence of non-uniformity of cells.

The battery module was manually assembled into a linear array of 6 cells, as shown in Fig. 1. The customized ceramic-fiberboard frame was used to hold battery cells and fix their position, which had a thickness of 10 mm and provided good electric and thermal insulation. The distance between adjacent batteries was 3 mm. Except for the ceramic frames on the top and bottom, nothing was filled in between cells. Two Al_2O_3 ceramic planes of 3-mm thick with 4 small screws and bolts were used to fix the battery module.

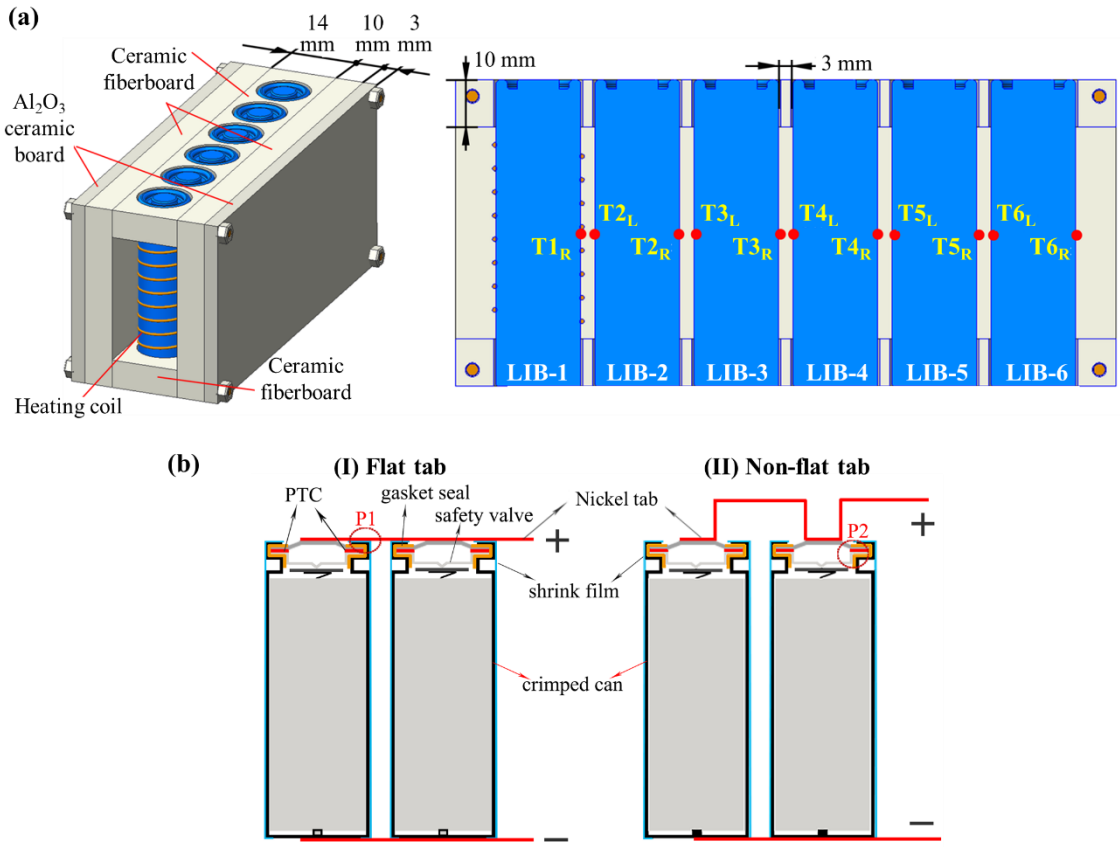

Fig. 1. Illustration of battery modules with six 18650 cells: (a) setup, dimension, and thermocouple locations, where the red points indicate the locations of thermocouples, and (b) two types of tabs to connect the top of the battery, (I) straight nickel tab, and (II) non-flat nickel tab.

2.2. Test procedure and parameters

The surface temperatures of all batteries were monitored with thermocouples attached on two sides of batteries at their half-height, as illustrated in Fig. 1a. The tiny K-type thermocouples with the 100-μm bead diameter were used. An electric resistance wire ($Cr_{20}Ni_{80}$) was convolved around battery No.1 (LIB-1) as the heat source to trigger the thermal runaway of LIB-1. The power of the electric resistance wire was controlled by a power regulator, which was set to 30 W for all tests. Once the thermal runaway

was initiated, the heating coil was turned off.

Ambient temperature (T_a). During tests, battery modules were placed in a thermostat (BTH-408C), which provides an isothermal environment of the designed temperature throughout the entire experiment. The mechanical ventilation within the thermostat was turned off to limited environmental airflow. Five different ambient temperatures, 20 ℃ (room temperature), 40 ℃, 50 ℃, 60 ℃, and 70 ℃ were examined.

SOC. Three battery SOCs of 30%, 70%, and 100% were varied. Before the test, all battery cells were charged to 100% SOC by the Constant Current-Constant Voltage method. Specifically, batteries were first charged in the constant current of 1075 mA until the cut-off voltage 4.2 V, and then charged in the constant voltage of 4.2 V until the current decreased to 107.5 mA. To obtain the required SOC, the cells were discharged in a constant current of 1075 mA.

Tab connection. Besides the open-circuit battery module, two parallel circuit-connection methods were also tested (Fig. 1b). Type-I connection used a flat nickel tab. This kind of connection is most used in EV battery modules, which has the merit of easy production but a high risk of the external short circuit. Type-II connection used a non-flat (step-shape) nickel tab, which occupies more space but lowers the risk of the external short circuit. Some EV battery modules also use the non-flat nickel tabs to connect batteries.

The real-time temperatures and voltages of each cell were monitored by a data logger (HIOKI LR8400) throughout the test. For each case, at least two repeating tests were conducted to reduce the random error, and the overall experimental repeatability was reasonable.

3. Results

3.1. Effect of ambient temperature

Figure 2 compares the battery surface temperature and voltage, tested under (a) room temperature at 20 ℃, and (b) above room temperature at 40 ℃ and 60 ℃. All battery cells were fully charged (SOC = 100%) without tab connections (i.e., open circuit). The photos of the battery module after thermal-runaway tests were also compared. At 20 ℃ (Fig. 2a), the voltage of the first cell (LIB-1) dropped down to 0.39 V after heating for 380 s, which indicated the failure of the battery cell. After another 126 s, the thermal runaway occurred, and then, the surface temperature rapidly raised to 603 ℃. At the same time, large quantities of gases ejected from the broken safety valve at high speed, which led to sparks and jet flame.

Note that the jet flame had no direct contact with nearby batteries, so the heat transfer to the adjacent battery (LIB-2) was mainly from the hot LIB-1. The surface temperature of LIB-2 near the first cell ($T2_L$) rapidly increased to 196 ℃ from 92 ℃. About 344 s after the failure of LIB-2, the voltage of LIB-2 also had a sudden drop, but the cell did not lead to the thermal runaway. The abnormal temperature increment to 430 ℃ was caused by the detachment of $T2_L$ and the contact with the hot LIB-1, evidenced by the slight increase of $T2_R$ on the other side. The peak temperature of the LIB-3 ($T3_L$) reached 164 ℃, about 500 s after the thermal runaway of LIB-1. Except for LIB-2 (failed but no thermal runaway), the other 4 cells were nearly not affected, which was proved by the post-test photo in Fig. 2a. Therefore, the thermal runway did not propagate to any cells at 20 ℃ with 100% SOC.

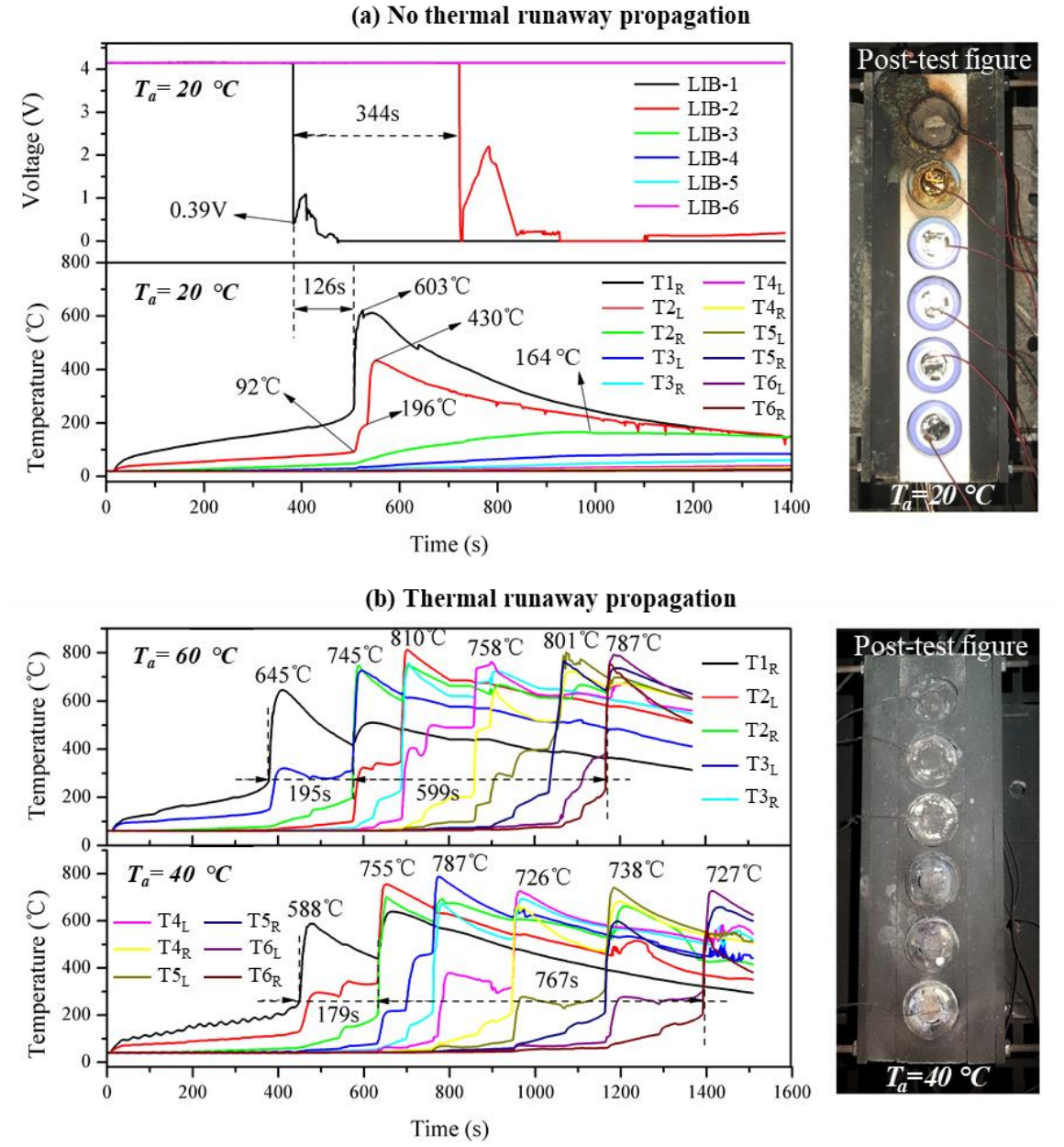

Fig. 2. The temperature and voltage evolution for the 100% SOC open-circuit battery module: (a) no thermal runaway propagation at the ambient temperature of 20 ℃, and (b) thermal runaway propagated at the ambient temperatures of 40 ℃ and 60 ℃.

At ambient temperatures of 40 ℃ and 60 ℃ with 100% SOC (Fig. 2b), the thermal runaway of 6 cells occurred in sequence. As influenced by the heating coil, $T1_R$, which was attached near the electrical resistance wire (see Fig. 1a), fluctuated during the initial heating. Eventually, the highest temperature of the LIB-1 was 588 ℃ and 645 ℃ at the ambient temperature of 40 ℃ and 60 ℃, respectively. In order to minimize the influence of ignition, LIB-1 was excluded from the analysis of the thermal-runaway propagation rate. Then, the total thermal-runaway propagation time from LIB-2 to LIB-6 was 767 s and 599 s at 40 ℃ and 60 ℃, respectively, with a reduced percentage of 21.9%. Therefore, thermal runaway propagates faster in this module at a higher ambient temperature. Additionally, the average peak temperature of batteries except the thermal runaway triggered one increased from 750 ℃ to 780 ℃ as the ambient temperature increased from 40 ℃ to 60 ℃. In short,

the probability and process of thermal-runaway propagation are closely related to the ambient temperature.

3.2. *Effect of SOC*

Figure 3 compares the battery surface temperature characteristics during the thermal-runaway propagation with different SOCs (30%, 70%, and 100%), where the ambient temperature was 60 ℃, and the circuit of the battery module was open. At SOC = 30% (Fig. 3a), the thermal runaway propagation was not initiated in the module. The peak surface temperature of the LIB-1 was only 406 ℃, and $T2_R$ only reached 154 ℃, which was much lower than the typical thermal- runaway temperature [3]. At SOC = 70% SOC (Fig. 3b), the total thermal-runaway propagation time from LIB-2 to LIB-6 was 764 s, which was 165 s (27.5%) longer than that with 100% SOC (Fig. 3c). Also, the average peak temperatures of batteries were 750 ℃ and 758 ℃ with 70% SOC and 100% SOC, respectively. Clearly, a higher SOC could lead to a severer thermal-runaway and a faster propagation.

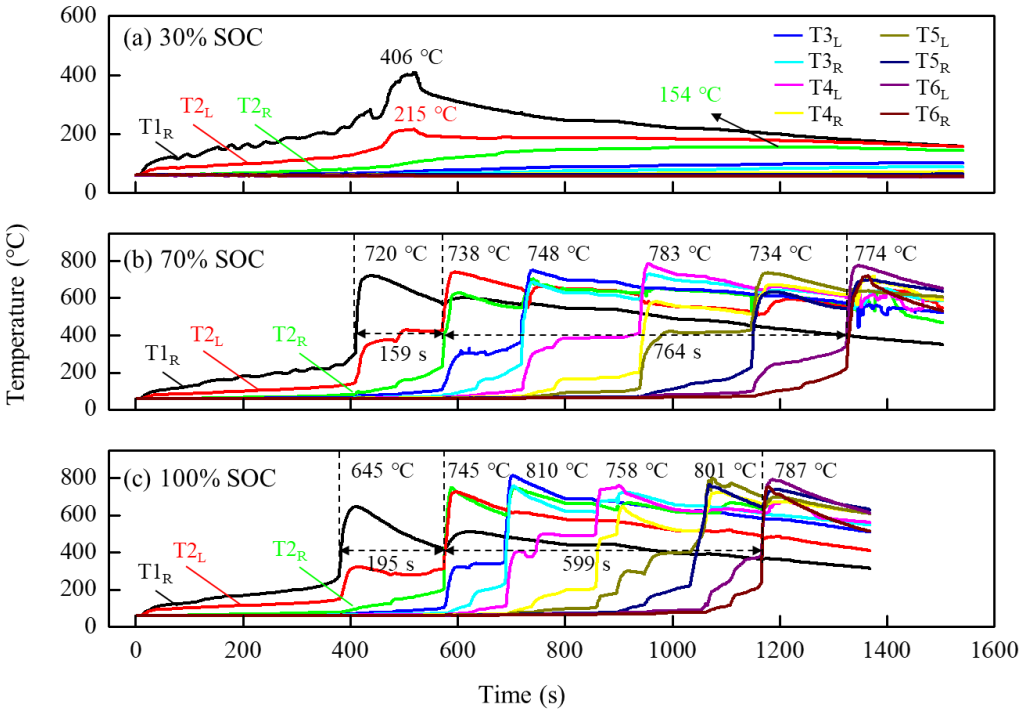

Fig. 3. Temperature curves at ambient temperature (T_a) of 60 ℃ for open-circuit battery module with (a) 30% SOC, (b) 70% SOC, and (c) 100% SOC.

3.3. *Effects of tab connections*

Figure 4(a) shows the battery surface temperatures with the SOC of 30% and the ambient temperature of 60 ℃, where the Type-I connection with flat tabs was used for the module. Compared to the open-circuit case in Fig. 3(a), the flat-tab connection also did not initiate thermal-runaway propagation. Nevertheless, the external short circuit was observed after the thermal-runaway of LIB-1, which caused the temperature raising of the other 5 cells from 62 ℃ to 154 ℃ in 30 s. The external short circuit resulted from Type-I parallel connection could be a result of the direct contact between positive nickel tab and steel shell, after the melting of heat-shrinkable films, as shown in Fig. 1b.

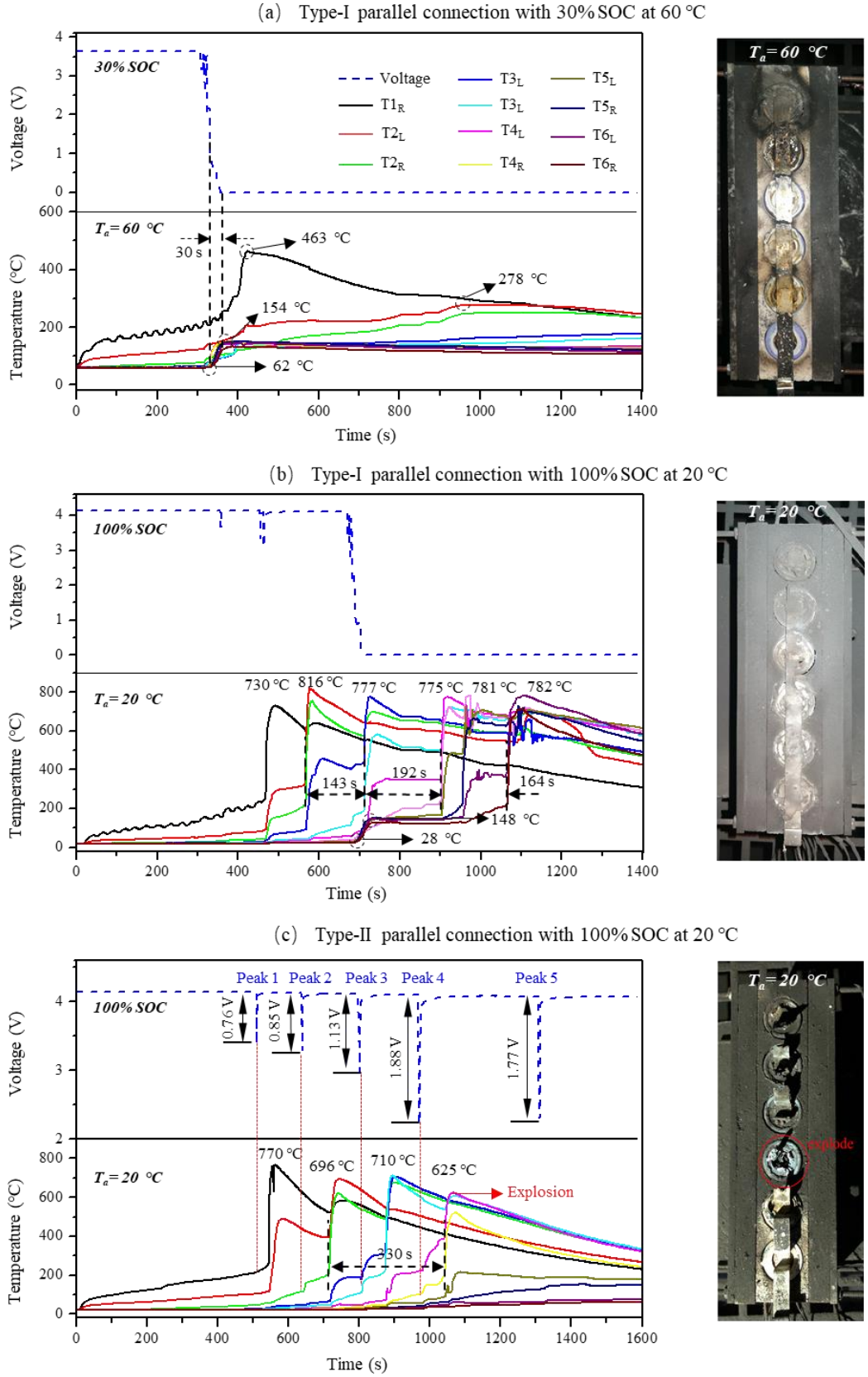

Fig. 4. Temperature curves, voltage evolution and post-test photos for the battery module with (a) 30% SOC in Type-I parallel connection at 60 °C, (b) 100% SOC in Type-I parallel connection at 20 °C, and (c) 100% SOC in Type-II parallel connection at 20 °C.

Considering the battery heat capacity (c_p) of 1243 J/(kg·K) from the adiabatic rate calorimeter (ARC) test and the battery mass (m) of 44.5 g, the heat released (Q_{es}) and the average self-heating power ($\dot{Q}_{es}$) due to the external short circuit could be estimated as

$$Q_{es} = \Delta \mathrm{SOC}_{es} E = c_b m_b (T_{es} - T_a), \qquad \dot{Q}_{es} = \frac{Q_{es}}{\Delta t} \tag{1}$$

where $\Delta \mathrm{SOC}_{es}$ is the change of SOC during the external short circuit, E = 28 kJ is the total electrical energy of the fully charged battery, c_b is the specific heat of battery, m_b is the mass of battery, T_{es} is the temperature after the external short circuit, and Δt is the time duration.

The calculated heat released was 5.1 kJ per cell, which was about 18% of the total electrical energy. In other words, the SOC of batteries decreases to about 12% after the external short circuit caused by the thermal-runaway of LIB-1. Note that the battery's internal temperature could be higher than the surface temperature, so the actual heat release and the decrease in SOC could be underestimated. In addition, the calculated average self-heating power of the external circuit was at least 170 W. Because internal electric resistance of the positive temperature coefficient (PTC) component increased rapidly to a tremendous value, and then the external short circuit current gradually decreased, the SOCs of other 5 cells did not decrease to zero immediately.

Figure 4(b) shows the thermal-runaway propagation with 100% SOC and the Type-I flat-tab parallel connection at the ambient temperature of 20 ℃. Compared to the failed thermal-runaway propagation for the open-circuit case with the same SOC and ambient temperature in Fig. 2(a), the thermal-runaway propagation occurred with the close circuit. The average thermal-runaway propagation rate was 0.42 #/min for the first 3 batteries (see more discussion in Section 4.2).

Moreover, right after the thermal-runaway of LIB-3, the external short circuit occurred, where the surface temperatures of LIB-4, 5, and 6 increased rapidly from 28 ℃ to 148 ℃. This process released at least 27% of the total electrical energy, that is, the SOC of these three batteries decreased to about 73%. After the external short circuit, the propagation rate increased by 20% to 0.50 #/min. Therefore, it is deduced that whether the circuit is open or closed for the battery module has a significant effect on the thermal-runaway propagation. In addition to the external short circuit and the consequent self-heating, the heat transfer through the nickel tab, as well as the internal short circuit, also contributes to the acceleration of thermal-runaway propagation.

Figure 4c shows the thermal-runaway propagation with 100% SOC and the non-flat-tab parallel connection at the same ambient temperature of 20 ℃. The Type-II connection prevents the direct contact of anode and cathode, thus, avoiding the external short circuit. Moreover, the voltage drop of one cell would not result in a voltage drop of other cells, so that only a temporary voltage drop can be observed. This could be caused by the short-time internal short circuit because its occurrence was accompanied with a temperature increase of a cell. As followed by the thermal-runaway propagation, nickel tabs broke down (see the photo in Fig. 4c) to break the battery from the module.

The internal short circuit of the thermal-runaway battery increased the overall current of the system. Thus, when the failure of the next cell occurred, the temporary voltage drop of the module during the internal short circuit continuously increased from 0.76 V (LIB-1) to 1.88 V (LIB-4). As every internal short circuit event gave a temperature rise to the remaining cells, the thermal-runaway process accelerated. The average thermal-runaway propagation rate was 0.36 #/min, which was slower than that with Type-I connection in Fig. 4b while faster than the open-circuit case in Fig. 2b with the ambient temperature of 40 ℃.

The thermal runaway of the battery could lead to an explosion, such as the LIB-4, which

characterized by the formation of a gap and dramatic venting (see the residue photo in Fig. 4c). After the explosion, the thermal-runaway propagation stopped. The peak temperature of LIB-4 was 625 ℃, which was lower than those of LIB-2 and LIB-3. The explosion was caused by a large quantity of ejected hot gases and particles that exceeded the design limit of safety vent. The explosion of LIB-4 was always observed in repeating tests. Therefore, Type-II non-flat tabs limit the external short circuit, but it may increase the risk of explosion, which needs further research.

4. Discussions

4.1. Critical thermal-runaway temperature

To characterize the thermal-runaway propagation, a critical thermal-runaway temperature (T_{crt}) can be used, which can be quantified through different standard tests. The most widely used method is ARC that gives a value of T_{crt} under the near adiabatic environment. However, the critical temperature from ARC cannot well characterize the thermal runaway in a real battery fire, because batteries are not heated uniformly and have a large temperature gradient. For example, in this experiment, the heating of the battery was one side, and the surface temperature difference between two sides of the cell could be up to 100 ℃. Therefore, we chose the surface temperature at the cold side as the critical thermal-runaway temperature (T_{crt}), which defined the lower limit for battery thermal runaway.

Figure 5 summarizes the critical thermal-runaway temperature varying with the ambient temperature and SOC, where the error bar shows the variation among 4 central cells from LIB-2 to LIB-5. LIB-1 was affected by the heating coil, and LIB-6 was exposed to the environment, so that they were not considered. It is apparent that the value of T_{crt} slightly increases with the ambient temperature. Specifically, for 100% SOC, T_{crt} increases from 209 ℃ to 225 ℃, as the T_a increases from 40 ℃ to 70 ℃. Moreover, T_{crt} of 100% SOC is lower than that of 70% SOC, and the temperature difference increases from 12 ℃ at T_a = 40 ℃ to 30 ℃ at T_a = 70 ℃. As expect, results indicate that batteries with a larger SOC have a higher risk of thermal runaway and fire.

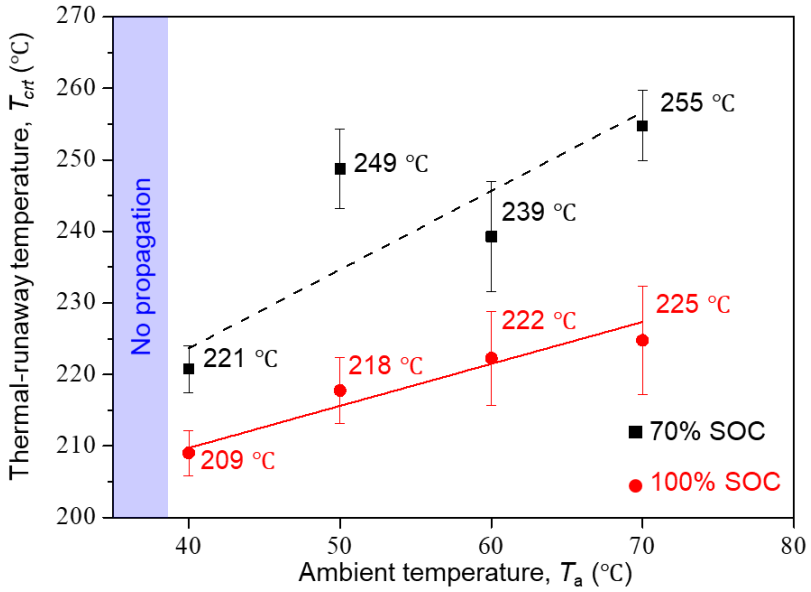

Fig. 5. The critical thermal-runaway temperature varying with the ambient temperature (T_a) and SOC.

4.2. Thermal-runaway propagation rate

For EVs and battery power storage units, there are thousands of battery cells to achieve the desired high voltage and energy capacity. In addition, to prevent the thermal runaway of each individual battery, it is more important to prevent the propagation of thermal runaway in the whole battery pack, which could cause disastrous fire accidents and severe threat to lives. In order to characterize the thermal-runaway propagation in the battery module, the average thermal-runaway propagation rate (or speed) from cell to cell, r [#/min], can be defined and measured from experiments as

$$r = \frac{n}{\Delta t} \tag{2}$$

where Δt [min] is the time of thermal-runaway propagation, and n [#] is the number of cells that were triggered to thermal-runaway.

Figure 6 summarizes the mean thermal-runaway speed (r) varying with the ambient temperatures (T_a) and SOC. Clearly, the thermal-runaway speed increases with SOC. Specifically, the increment of r is about 15%, as SOC increases from 70% to 100%. Moreover, as the ambient temperature increases from 40 °C to 70 °C, the average thermal-runaway speed is accelerated by 54% from 0.31 to 0.48 #/min with 100% SOC. In the meantime, the thermal-runaway propagation rate is increased by 80% from 0.25 to 0.45 #/min with 70% SOC. In other words, the thermal runaway of cells propagates faster at higher ambient temperature, and the influence of ambient temperature can exceed that of SOC.

Figure 7 illustrates the propagation of thermal runaway in the linear battery module. Except for LIB-1, the thermal runaway of all other cells could be triggered by the cell on the left. Thermal-runaway propagation of LIBs relies on heat transfer from cell to cell. The propagation from LIB-1 to LIB-2 is controlled by the heating coil. The heating coil can heat LIB-1 above 800 °C, which is higher than the maximum temperature caused by self-heating. Thus, if the thermal runaway of LIB-2 cannot be initiated with given SOC and ambient temperature, it is also impossible for a thermal runaway to propagate between the remaining cells.

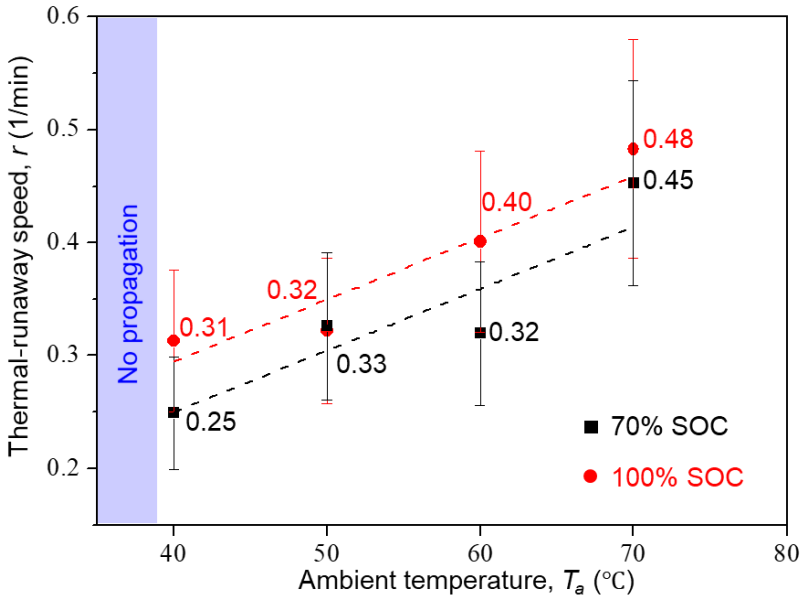

Fig. 6. Thermal-runaway propagation rate of battery modules (r) varying with the ambient temperature (T_a) and SOC.

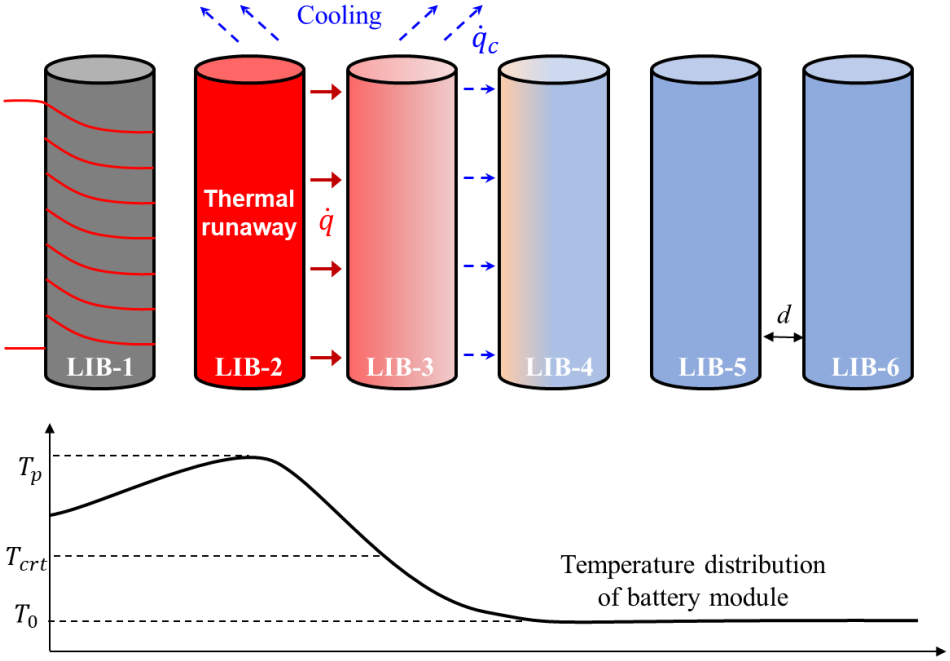

Fig. 7. The illustration of the thermal-runaway propagation in a linear array of the LIB module.

The propagation of thermal runaway can be analogized to the fire spread. Thus, the propagation rate is controlled by the ratio between the heat transfer between cells (driven force) and the thermal inertia of cell (resistance) [21, 22]. As a first approximation, the temperature gradient inside the battery cell is ignored, so the propagation rate may be expressed as

$$r \approx \frac{\dot{q} - \dot{q}_c}{m_b c_b (T_{crt} - T_0)} \approx \frac{h_{TR} A (T_p - T_{crt}) - h_c A (T_{crt} - T_a)}{m_b c_b (T_{crt} - T_0)} \tag{3}$$

Considering the thermal runaway propagating from LIB-2 to LIB-3 in Fig. 7, $\dot{q} = h_{TR} A (T_p - T_{crt})$ is the effective heat transfer between thermal-runaway cell (LIB-2) and the next cell (LIB-2), which includes convection and radiation, as well as, the conduction through tabs; h_{TR} is the overall coefficient of heating; $A = A_b/2$ is the half of cell surface area; $\dot{q}_c = h_c A (T_{crt} - T_a)$ represents the cooling by the environment and LIB-4; and h_c is the overall cooling coefficient. The peak temperature after the thermal runaway (T_p) depends on the original SOC and should satisfy

$$\mathrm{SOC} \cdot E = c_b m_b (T_p - T_a) \tag{4}$$

which neglects the cooling effect because of the rapid thermal-runaway process. The original battery temperature (T_0) depends on the ambient temperature and external short circuit, as shown in Eq. (1).

Thus, the thermal-runaway propagation rate becomes

$$r \approx \frac{\mathrm{SOC}\left(\frac{E}{m_b c_b}\right) h_{TR} A - (h_{TR} A + h_c A)(T_{crt} - T_a)}{m_b c_b (T_{crt} - T_a) - Q_{es}} \tag{5}$$

which gives a qualitative description of all influence factors in this work. Specifically, the thermal-runaway propagation rate increases as the SOC or ambient temperature (T_a) increases whereas it decreases with the reducing heat transfer coefficient between battery cells (h_b), as demonstrated in Fig. 6. The increase of the ambient temperature (T_a) both decrease the denominator and increase the numerator, so that its acceleration

effect on thermal runway seems to exceed the increase of SOC.

Additionally, the existence of an external short circuit (Q_{es}) preheats all batteries that are still connected to the module, thus, increasing the propagation rate. For example, the thermal-runaway speed in a battery module with 100% SOC and Type-I connection at $T_a = 20$ °C (Fig. 4b) is 0.6 #/min after the external short circuit, which is 1.5 times as fast as that of the open-circuit case in Fig. 2b even when the ambient temperature increased to 40 °C. Moreover, the heat transfer coefficient between battery cells (i.e., both h_{TR} and h_c) decreases with the distance between adjacent cells, but increases if tabs are used to connect the battery module. This could be the reason why the parallel-connected battery modules usually present a higher thermal-runaway propagation risk.

Moreover, for any given configuration of the linear battery module, Eq. (5) further defines the minimum values of ambient temperature ($T_{a,min}$) and $\mathrm{SOC}_{\min}$ for the thermal-runaway propagation ($r = 0$), as

$$\mathrm{SOC}_{min} \approx \left(1 + \frac{h_c}{h_{TR}}\right)\frac{m_b c_b (T_{crt} - T_a)}{E} \tag{6a}$$

$$T_{a,min} \approx T_{crt} - \frac{\mathrm{SOC} \cdot E}{m_b c_b}\left(\frac{h_{TR}}{h_{TR} + h_c}\right) \tag{7a}$$

which also qualitatively explains why the thermal-runaway propagation cannot take place when the SOC and ambient temperature are low.

When the gap between battery cells are small or well contacted with each other, the value of h_{TR} reaches the maximum and comparable to h_c, that is, $h_{TR} \approx h_c$. Then, we can get the lower limit of minimum thermal-runaway conditions

$$\mathrm{SOC}_{min} \geq \frac{2m_b c_b (T_{crt} - T_a)}{E} \qquad (h_{TR} \approx h_c) \tag{6b}$$

$$T_{a,min} \geq T_{crt} - \frac{\mathrm{SOC} \cdot E}{2m_b c_b} \qquad (h_{TR} \approx h_c) \tag{7b}$$

This suggests that when all electrical energy of one cell is released as heat, it should, at least, heat two cells from the ambient temperature up to the critical thermal-runaway temperature, as expected.

On the other hand, when the gap between battery cells are too large ($h_{TR} \ll h_c$), we have

$$\mathrm{SOC}_{min} > 100\% \qquad (h_{TR} \ll h_c) \tag{6c}$$

$$T_{a,min} \to T_{crt} \qquad (h_{TR} \ll h_c) \tag{7d}$$

where the minimum ambient temperature needs to approach the critical thermal-runaway temperature of the battery, and the value of SOC becomes less relevant to the probability of the thermal-runaway propagation.

5. Conclusions

In this work, the characteristics of thermal-runaway propagation in linear-arranged 18650 cylindrical lithium-ion battery modules with 3-mm gap, three states of charge (30%, 70%, and 100% SOCs), three connection methods (open-circuit, flat-tab, and non-flat-tab parallel connection), and ambient temperatures from 20 °C to 70 °C. Results indicate that the thermal-runaway propagation speed was about 0.35 ± 0.15 #/min, which increased with SOC and ambient temperature. Specifically, the increment of the thermal-runaway propagation rate is about 15%, as the SOC increases from 70% to 100%, and about 50%, as the ambient temperature increases from 40 °C to 70 °C.

The critical surface temperature of thermal runaway ranged from 209 ℃ to 245 ℃, which increased with ambient temperature while decreased with SOC. Compared to the open-circuit module, the flat tab connection could cause an external short circuit to accelerate the thermal-runaway propagation, and the non-flat tab connection was more likely to trigger an explosion. A heat transfer analysis was proposed to qualitatively explain the speed and limiting conditions of thermal-runaway propagation, as well as, the influence of SOC, ambient temperature, and tab connection. This work reveals the thermal-runaway propagation characteristics under well-controlled environments, which could provide scientific guidelines to improve the safety of the battery module and reduce battery fire hazards.

Acknowledgment

This work is supported by the National Key R&D Program of China (2018YFB0104100).

References

1. Feng X, Ouyang M, Liu X, et al (2018) Thermal runaway mechanism of lithium ion battery for electric vehicles: A review. Energy Storage Mater 10:246–267. https://doi.org/10.1016/j.ensm.2017.05.013
2. Wang Q, Ping P, Zhao X, et al (2012) Thermal runaway caused fire and explosion of lithium ion battery. J Power Sources 208:210–224. https://doi.org/10.1016/j.jpowsour.2012.02.038
3. Wang Q, Mao B, Stoliarov SI, Sun J (2019) A review of lithium ion battery failure mechanisms and fire prevention strategies. Prog Energy Combust Sci 73:95–131. https://doi.org/10.1016/j.pecs.2019.03.002
4. Niu HC, Li Z (2018) Application of RAC Method in Fire Risk Assessment of Lithium-ion Battery Factories. Procedia Eng 211:1115–1119. https://doi.org/10.1016/j.proeng.2017.12.117
5. Sun P, Bisschop R, Niu H, Huang X (2020) A Review of Battery Fires in Electric Vehicles. Springer US
6. Liu X, Wu Z, Stoliarov SI, et al (2016) Heat release during thermally-induced failure of a lithium ion battery: Impact of cathode composition. Fire Saf J 85:10–22. https://doi.org/10.1016/j.firesaf.2016.08.001
7. Meligrana G, Lueangchaichaweng W, Colò F, et al (2017) Gallium oxide nanorods as novel, safe and durable anode material for Li- and Na-ion batteries. Electrochim Acta 235:143–149. https://doi.org/10.1016/j.electacta.2017.03.047
8. Zheng S, Wang L, Feng X, He X (2018) Probing the heat sources during thermal runaway process by thermal analysis of different battery chemistries. J Power Sources 378:527–536. https://doi.org/10.1016/j.jpowsour.2017.12.050
9. Wang Q, Jiang L, Yu Y, Sun J (2019) Progress of enhancing the safety of lithium ion battery from the electrolyte aspect. Nano Energy 55:93–114. https://doi.org/10.1016/j.nanoen.2018.10.035
10. Said AO, Lee C, Stoliarov SI, Marshall AW (2019) Comprehensive analysis of dynamics and hazards associated with cascading failure in 18650 lithium ion cell arrays. Appl Energy 248:415–428. https://doi.org/10.1016/j.apenergy.2019.04.141
11. Ouyang M, Zhang M, Feng X, et al (2015) Internal short circuit detection for battery pack using equivalent parameter and consistency method. J Power Sources 294:272–283. https://doi.org/10.1016/j.jpowsour.2015.06.087

12. Shang Z, Qi H, Liu X, et al (2019) Structural optimization of lithium-ion battery for improving thermal performance based on a liquid cooling system. Int J Heat Mass Transf 130:33–41. https://doi.org/10.1016/j.ijheatmasstransfer.2018.10.074
13. Yan J, Wang Q, Li K, Sun J (2016) Numerical study on the thermal performance of a composite board in battery thermal management system. Appl Therm Eng 106:131–140. https://doi.org/10.1016/j.applthermaleng.2016.05.187
14. Liu Y, Sun P, Niu H, et al (2020) Propensity to self-heating ignition of non-operating pouch Lithium-ion battery pack on a hot boundary. Fire Saf J
15. Feng X, Sun J, Ouyang M, et al (2015) Characterization of penetration induced thermal runaway propagation process within a large format lithium ion battery module. J Power Sources 275:261–273. https://doi.org/10.1016/j.jpowsour.2014.11.017
16. Lopez CF, Jeevarajan JA, Mukherjee PP (2015) Experimental Analysis of Thermal Runaway and Propagation in Lithium-Ion Battery Modules. J Electrochem Soc 162:A1905–A1915. https://doi.org/10.1149/2.0921509jes
17. Huang P, Chen H, Verma A, et al (2019) Non-dimensional analysis of the criticality of Li-ion battery thermal runaway behavior. J Hazard Mater 369:268–278. https://doi.org/10.1016/j.jhazmat.2019.01.049
18. Gao S, Feng X, Lu L, et al (2019) An experimental and analytical study of thermal runaway propagation in a large format lithium ion battery module with NCM pouch-cells in parallel. Int J Heat Mass Transf 135:93–103. https://doi.org/10.1016/j.ijheatmasstransfer.2019.01.125
19. Lamb J, Orendorff CJ, Steele LAM, Spangler SW (2015) Failure propagation in multi-cell lithium ion batteries. J Power Sources 283:517–523. https://doi.org/10.1016/j.jpowsour.2014.10.081
20. Zhong G, Li H, Wang C, et al (2018) Experimental Analysis of Thermal Runaway Propagation Risk within 18650 Lithium-Ion Battery Modules. J Electrochem Soc 165:A1925–A1934. https://doi.org/10.1149/2.0461809jes
21. Emmons HW (1963) Fire in the forest. Fire Res Abstr Rev 5:163–178. https://doi.org/10.17226/18854
22. Williams FA (1977) Mechanisms of fire spread. Symp Combust 16:1281–1294. https://doi.org/10.1016/S0082-0784(77)80415-3